

RSC Advances



This is an *Accepted Manuscript*, which has been through the Royal Society of Chemistry peer review process and has been accepted for publication.

Accepted Manuscripts are published online shortly after acceptance, before technical editing, formatting and proof reading. Using this free service, authors can make their results available to the community, in citable form, before we publish the edited article. This *Accepted Manuscript* will be replaced by the edited, formatted and paginated article as soon as this is available.

You can find more information about *Accepted Manuscripts* in the [Information for Authors](#).

Please note that technical editing may introduce minor changes to the text and/or graphics, which may alter content. The journal's standard [Terms & Conditions](#) and the [Ethical guidelines](#) still apply. In no event shall the Royal Society of Chemistry be held responsible for any errors or omissions in this *Accepted Manuscript* or any consequences arising from the use of any information it contains.

Antisite defects in LiCoPO₄ nanocrystals synthesized via supercritical fluid process

Murukanahally Kempaiah Devaraju*[†], Quang Duc Truong[†], Takaaki Tomai[†], Hiroshi Hyodo[†], Yoshikazu Sasaki[‡] and Itaru Honma*[†]

[†] Institute of Multidisciplinary Research for Advanced Materials, Tohoku University, Katahira 2-1-1, Aoba-ku, Sendai 980-8577, Japan.

[‡]DATUM Solution Business Operations, JEOL, Ltd., Tokyo 196-0022, Japan.

Corresponding authors: M K Devaraju (devaraju113@gmail.com) and I. Honma (i.honma@tagen.tohoku.ac.jp)

LiCoPO₄ nanocrystals are synthesized via supercritical fluid process at 380 °C for 1h and we visualize Li/Co antisite defects along two crystallographic directions using annular dark and bright field scanning transmission electron microscopy (STEM). The antisite defects are observed with bright/dark contrast produced by Co atoms in Li columns in both HAADF (high angle annular dark field) and ABF (annular bright field) images viewed along [010] directions. Interestingly, few antisite defects are observed along [101] directions with weak contrast and P atoms are observed near to Co atoms.

1. Introduction

The structural observations of energy materials at atomic scale are very important to understand the crystallographic stability upon charge/discharge process and the reason for the capacity fading. The point defects in energy materials affect the ordered arrangement of atoms, mass and charge transport behaviors.¹ Recently, study of point defects such as vacancies, dopants and antisite defects in inorganic crystals, layered oxides and olivine structured lithium metal phosphates using various techniques have been an interesting topic.² However, the atomic scale visualization of antisite defects in olivine structured lithium metal phosphates using aberration-corrected scanning transmission electron microscopy (STEM) along with progress in the Z-contrast technique is limited.³

Among lithium metal phosphates, LiFePO₄ and LiMnPO₄ have been extensively studied for the application

in lithium ion batteries.⁴ Recently, LiCoPO_4 is considered as an interesting alternative cathode material because of its high energy density and large theoretical capacity of 167 mA h g^{-1} . However, the practical use of LiCoPO_4 is not possible due to its poor cycling performances because of low electronic conductivity and limited lithium diffusion and other factors.⁵ Therefore, it is necessary to understand the possible reason for the poor cycling performances of bulk/nanosize LiCoPO_4 cathode materials. Recently, our group reported atomic scale visualization of $\text{Li}_2\text{CoSiO}_4$ nanomaterials synthesized via supercritical fluid process⁶ and direct observation of antisite defects along [010] direction in LiCoPO_4 material synthesized via sol-gel route.^{5c, 7}

Herein, we report atomic scale visualization of antisite defects in LiCoPO_4 along two zone directions and favorable arrangement of antisite defects along *b*-axis [010] in LiCoPO_4 nanocrystals synthesized using $\text{CoCl}_2 \cdot 6\text{H}_2\text{O}$, *o*- H_3PO_4 and $\text{LiOH} \cdot \text{H}_2\text{O}$ as starting materials via supercritical fluid process at $380 \text{ }^\circ\text{C}$ for 1h.

2. Experimental section

LiCoPO_4 nanocrystals were synthesized from $\text{CoCl}_2 \cdot 6\text{H}_2\text{O}$, (Wako, Japan) *o*- H_3PO_4 (Wako, Japan) and $\text{LiOH} \cdot \text{H}_2\text{O}$ (Wako, Japan) in 1:1:1 molar ratio. Oleylamine (Wako, Japan) was used both as surfactant and reducing agent. First, $\text{CoCl}_2 \cdot 6\text{H}_2\text{O}$ was dissolved in a solution of water-ethanol mixed solvents (1:1 volume ratio) and H_3PO_4 solution was added slowly with constant stirring followed by addition of lithium acetyl acetate after that oleylamine (metal ion to surfactant 1:20) was added. The solution mixture was stirred for about 20 min after that 5 ml solution (50% fill) was transferred to batch reactors (total 4 reactors, each 10 ml volume). The batch reactors were heated at $380 \text{ }^\circ\text{C}$ for 1 h and then reactors were quenched in cold water. The products were recovered by washing and dried in a vacuum for overnight.

2.1. Material characterization

The powder X-ray diffraction (XRD) analysis was carried out using a Bruker AXS D8 Advance instrument with $\text{Cu K}\alpha$ radiation. The morphology and size of the particles were determined using high-resolution transmission electron microscopy, Annular bright field images (ABF) and high angle

annular dark field (HAADF) images, elemental mapping and energy dispersive spectroscopy (EDS) were observed using JEM-2010F at 200 keV. The crystal structures model were drawn by VESTA.¹²

3. Results and discussion

3.1. Observation of antisite defects along [010] direction

LiCoPO₄ material is less studied in terms of crystal structure analysis and for electrochemical applications when compared to LiFePO₄ material. Fig. 1a shows the crystal structure model of LiCoPO₄, the structure is formed by composing of a chain of distorted CoO₆ octahedral which are cross linked with PO₄ tetrahedra with edge and corner sharing of oxo-anions. LiCoPO₄ crystal structure was viewed along [010] direction, where the position of Co, P, O and Li atoms can be seen. Li atoms located at M1 sites and Co atoms located at M2 sites, this model is useful for the identification of Li/Co antisite defects in LiCoPO₄ material. Fig. 1b and c show the high angle annular dark-field (HAADF) scanning transmission electron microscopy (STEM) and annular bright/dark field (ABF) scanning transmission electron microscopy (STEM) images of LiCoPO₄ nanocrystals along [010] direction. The bright/dark contrast produced by Co sites can be clearly observed in both HAADF and ABF STEM images as shown in Fig. 1b and 1c. P sites can be seen adjacent to each Co sites with weaker contrast than the Co columns. Although, HAADF-STEM technique has the advantage for direct identification of atomic columns but O and Li sites are not visible because their specific physical properties which are not enough to produce visible contrast. The contrast from ADF image is roughly correlated with the atomic number according to a $Z^{1.7}$ relationship.⁸ Hence, Li atoms ($Z=3$) are invisible even at the high resolution mode.

In addition, some of O columns are overlapped with Co and P columns along [010] direction as shown in Fig. 1b, this observation also reported by Ikuhara et al.^{8a} In our investigation, we observed few O atoms near to Co and P atoms with weak contrast (please see enlarged portion of Fig. S1). On the enlarged STEM image, two dimensional atom arrays are superimposed as shown in enlarged image in Fig. 1b and c for direct comparison of unit cell atomic arrangement in LiCoPO₄ nanocrystals. However, the superimposed arrays are not well fitted with the image, because of structural distortion of LiCoPO₄ nanocrystals, which is mainly depends on synthesis procedure, we can suspect that, the nanosize particles

may have crystal distortion than the bulk particles.⁷ Co and P atomic columns are not independently resolved due to the short distance between the atoms but they appeared as hexagonal shape which is matched well with the illustrations shown in Fig. 1b. Since, Li sites are not visible in HAADF mode, the strong contrast observed in Fig. 1b revealed that Li columns have been occupied by Co atoms as shown in Fig. 1b and c.

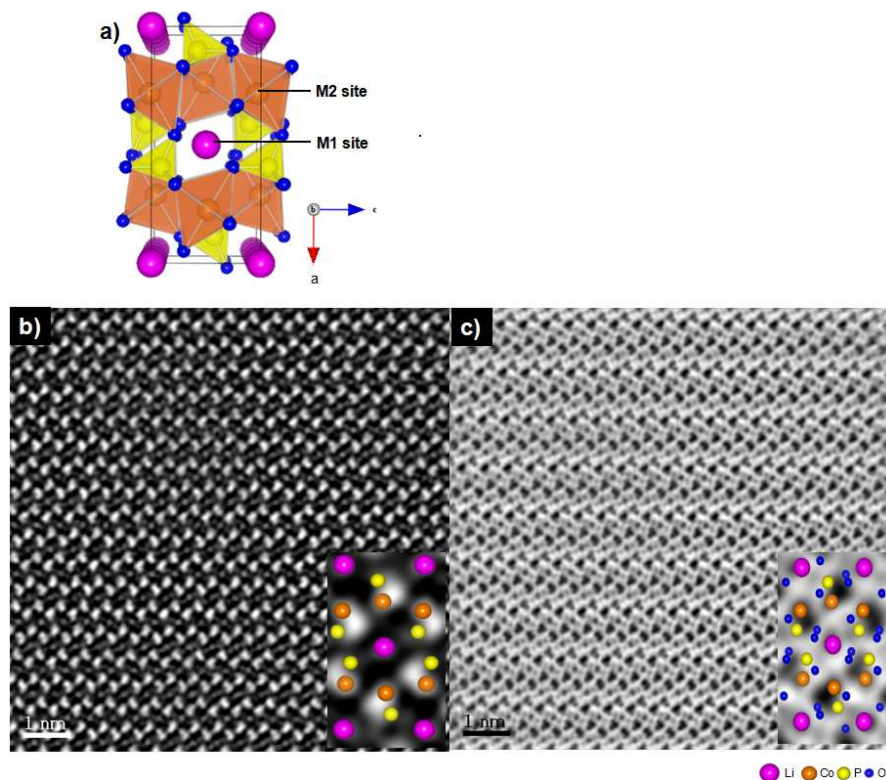


Fig. 1 (a) Crystal structure of LiCoPO_4 viewed along $[010]$ direction. (b) HAADF STEM image viewed along $[010]$ direction, the enlarged image with superimposed atomic arrays shows the position of atoms in LiCoPO_4 ; circle shows the Co cations as antisite defects in lithium site and c) ABF STEM image viewed along $[010]$ direction, the enlarged image with superimposed atomic arrays shows the position of atoms in LiCoPO_4 , circle shows the Co cations as antisite defects in lithium site.

The observed strong contrast clearly indicate the Li to Co exchange antisite defects in LiCoPO_4 nanocrystals synthesized via supercritical fluid process. The cation exchange is intensive and exchanged in crystal planes of LiCoPO_4 nanocrystals, the ratio of cation exchange in LiCoPO_4 differs from LiFePO_4 and LiMnPO_4 material⁹ due to the behavior of cation in that particular crystal symmetry. The close observation

in ABF image, we can see Li atoms in Co sites, it is confirmed because of weak contrast produced by Co sites (supporting information (Fig. S1)). These observations clearly indicate the crystallographic disorder in the form of antisite defects in LiCoPO₄ nanocrystals.

3.2. Observation of antisite defects along [101] direction

Fig. 2a shows the crystal structure model of LiCoPO₄ observed along [101] direction. Fig. 2a and b shows the high angle annular dark-field (HAADF) scanning transmission electron microscopy (STEM) and annular bright field (ABF) scanning transmission electron microscopy (STEM) images of LiCoPO₄ nanocrystals along [101] zone direction. The large scale ADF and ABF images are shown in Fig. S1. The bright/dark contrast produced by Co atoms along [101] directions in LiCoPO₄ nanocrystals can be clearly seen in Fig. 2b and 2c. The exchange of Li atoms by Co atoms is observed in very few Li site along this direction, the inhomogeneous lithium columns intensities in STEM along the [101] direction may indicate that the preferential arrangement of antisite cobalt cations along the [010] directions. We obtained multiple HAADF images and observed around 442 columns in which visible contrast at lithium site was observed in 10 columns.

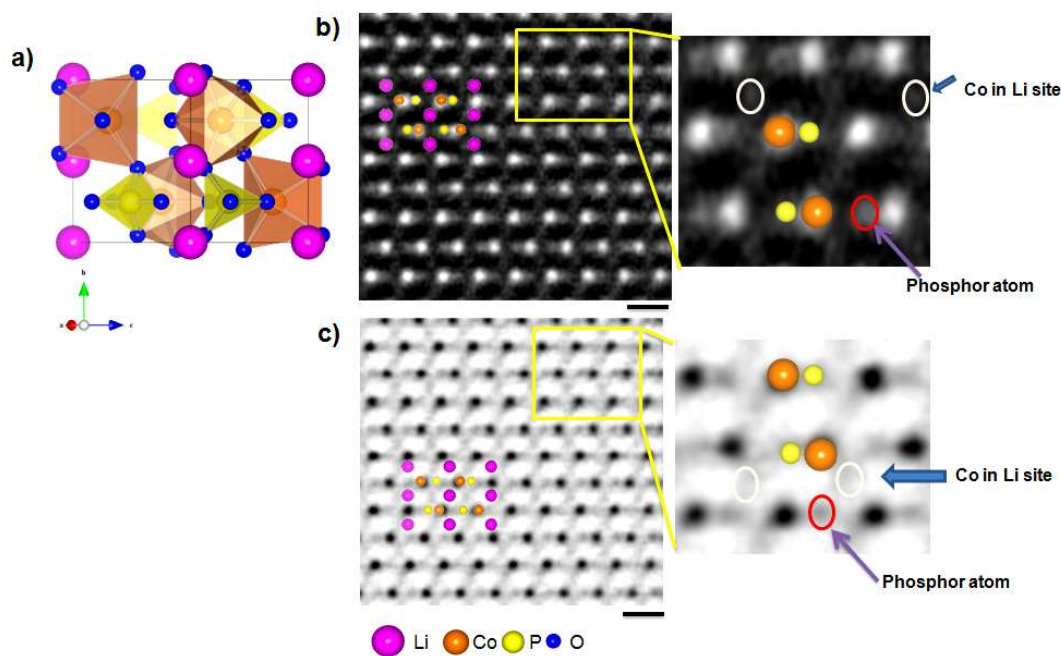


Fig. 2(a) Crystal structure of LiCoPO₄ viewed along [101] direction. (b) HAADF STEM image viewed along [101] direction, the inset is the superimposed atomic arrays which show the position of atoms in

LiCoPO₄ and (c) ABF STEM image viewed along [101] direction, the inset is the superimposed atomic arrays which show the position of atoms in LiCoPO₄; antisite defects with weak contrast can be seen (please see the circle mark, please see supporting information also). The scale bar is 5 Å.

The absence of antisite defects of Li columns along [001] direction is reported by Ikuhara et al.^{3a} The contrast of P atoms is dimmed due to high contrast produced by Co atoms, however P atoms with weak contrast adjacent to Co atoms can be observed (please see enlarged portion in Fig. 2, and supporting information (Fig. S2)). The inset in Fig. 2a and 2b shows the superimposed two dimensional atomic arrangements for better view of atoms in STEM images. The reason for the antisite arrangement along [010] direction is that, the transport behavior of the lithium ions¹⁰ which suggest that the lowest activation barrier lies along the *b* axis reported for LiFePO₄ material,^{10a, e, f} similar results can be expected for LiCoPO₄ cathode material.

3.3. Arrangement of antisite defects in LiCoPO₄ nanocrystals

Fig. 3 shows the schematic illustrations of the arrangement of antisite defects along [010], and [101] zone directions.

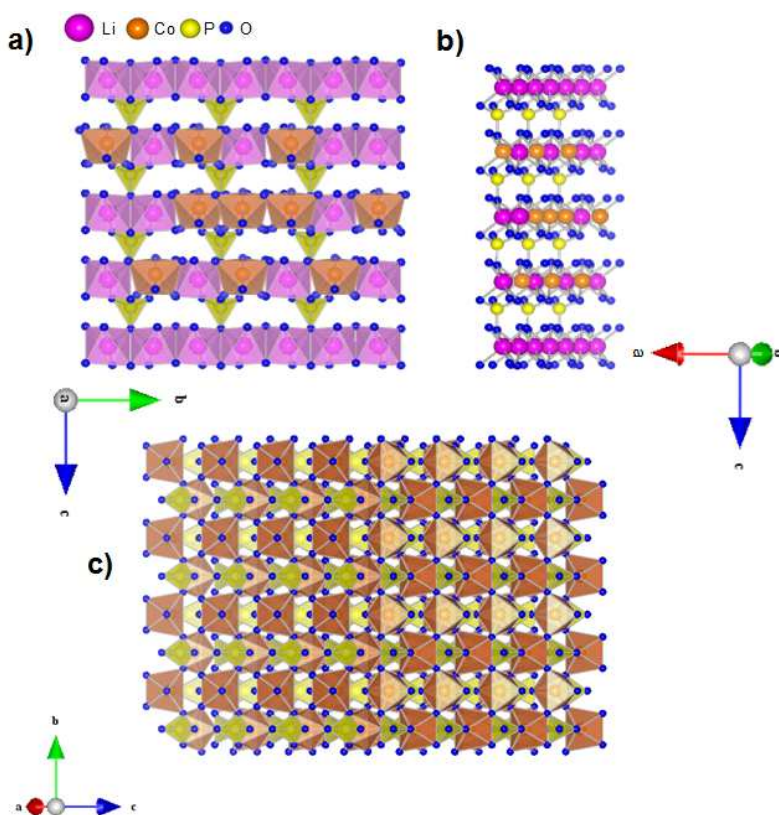


Fig. 3 Schematic illustrations showing the arrangement of antisite cobalt cations. a) Two dimensional projection along [010] direction. b) Three dimensional projection showing antisite defects along [010] direction and c) Two dimensional projection showing P atoms near to Cobalt atoms of along [101] direction. Some atoms are omitted for clarity.

In Fig. 3a and 3b, we can see the lithium ions in M1 site and few cobalt atoms in M1 site as antisite defects. In the olivines structure lithium ions in M1 site and they are edge-sharing, the distance between the neighboring cations in the M1 site is shorter than the cations in M2 site which are corner sharing. This structural arrangements lead to distorted shape of the oxygen octahedral for the M1 sites to minimize the electrostatic repulsion between the cations.^{4a} In LiCoPO_4 , M1 site is occupied by cobalt ions, the structural instability will be resulted due to the difference in valence number which creates electrostatic repulsion.^{3a} The phosphor atoms which are adjacent to Co atoms can be observed (See the circle mark in enlarged portion of Fig. 2). This indicated that P atoms can be observed along [101] zone direction. Further, the two-dimensional projection shown in Fig. 3c shows the presence of P atoms near to cobalt atoms along [101] zone directions, which is matched well with the ADF and ABF image along [101] directions shown in Fig. 2b and Fig. S2.

3.4. Crystallinity and morphological analysis

Fig. 4 shows the XRD, TEM, ED and HRTEM image of LiCoPO_4 nanocrystals synthesized via supercritical fluid process. The XRD patterns shows well developed diffraction peaks which can be indexed to orthorhombic crystal system with $Pnma$ space group. The calculated cell parameters are $a=10.2901 \text{ \AA}$, $b=5.9901 \text{ \AA}$ and $c=4.7001$, which are almost consistent with the reported values.¹¹ The pattern exhibited no impurities and suggests the obtained product is a single phase material. Further, the morphology of the synthesized product was observed by TEM analysis, the particles showed mixed rod and plate like morphologies with 200-250 nm in diameter and 400-800 nm in length for rod like particles (see supporting information, Fig. S1). Plate like particles showed 250-400 nm in length and width, and side thickness below 20 nm, which is along the b-axis as shown in Fig. 3b (supporting information Fig. S3). The ED pattern taken

along [010] zone axis shown in Fig. 4c indicates the single crystalline nature of LiCoPO₄ particles and HRTEM image shown in Fig. 4d exhibits well resolved lattice fringes, where lattice fringes on a and c plane can be seen. The purity of the LiCoPO₄ nanocrystals was further characterized by EDS analysis shown in Fig. S4 (supporting information). The homogeneous distribution of Co, O and P can be seen in elemental mapping by STEM analysis. The identification of Co, O and P can be seen in EDS spectra. The results suggest the purity of the LiCoPO₄ nanocrystals.

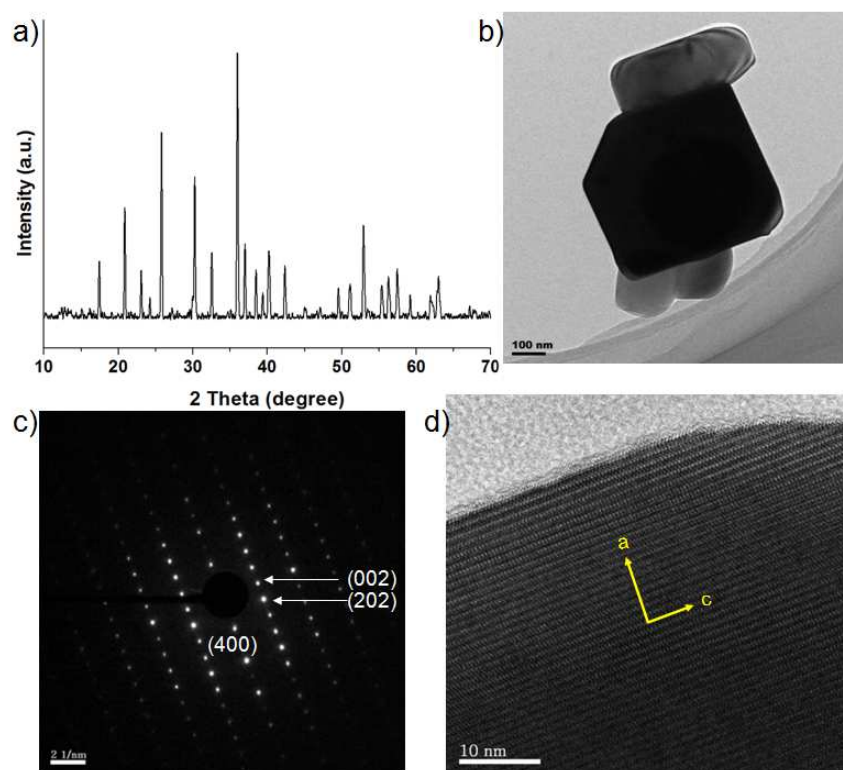


Fig. 4(a) XRD pattern of LiCoPO₄ nanocrystals synthesized via supercritical fluid process at 380 °C for 1h. (b) TEM image of LiCoPO₄ nanocrystals. (c) ED pattern and d) HRTEM image.

4. Conclusions

In conclusion, we have demonstrated the Co antisite defects are presented in LiCoPO₄ nanocrystals synthesized via supercritical process at 380 °C for 1h. Investigation of antisite defects along [010] and [101] directions were demonstrated, HAADF and ADF analysis showed more antisite arrangements along [010] direction and few antisite defects along [101] directions. Few oxygen atoms are also observed along [010] direction. Phosphor atoms which are neighbor to Co atoms were also identified along [101] directions. To

best of our knowledge, first time we show the antisite defects along two zone directions. Phosphor and oxygen atoms were also observed using HAADF and ABF images.

Acknowledgements

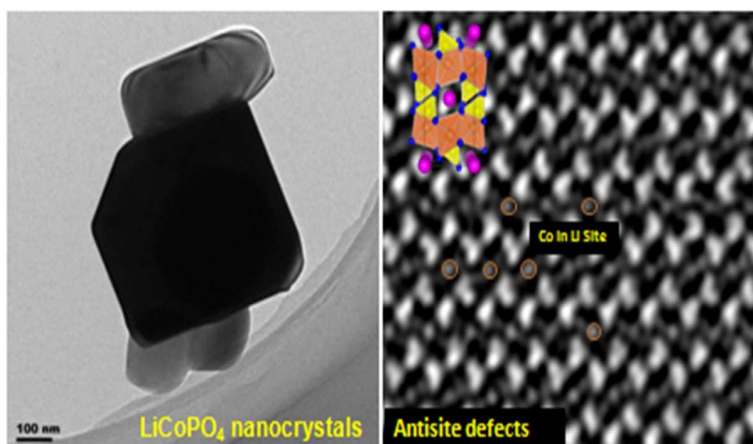
This work was supported by the Funding Program for World-Leading Innovative R&D on Science and Technology (FIRST), ‘Innovative Basic Research Toward Creation of High-Performance Battery’, from the Cabinet Office of Japan and the Japan Society for the Promotion of Science (JSPS).

Notes and references

- 1 (a) G. Hammerl, A. Schmehl, R.R. Schulz, B. Goetz, H. Bielefeldt, C.W. Schneider, H. Hilgenkamp, J. Mannhart, *Nature*, 2000, **407**, 162; (b) J.P. Buban, K. Matsunaga, J. Chen, N. Shibata, W.Y. Ching, T. Yamamoto, Y. Ikuhara, *Science*, 2006, **311**, 212; (c) Y. Sato, J. P. Buban, T. Mizoguchi, N. Shibata, M. Yodogawa, T. Yamamoto, Y. Ikuhara, *Phys. Rev. Lett.*, 2006, **97**, 106802.
- 2 (a) C. M. B. Henderson, K. S. Knight, S. A. T. Redfern, B. J. Wood, *Science*, 1996, **271**, 1713; (b) D. J. Norris, A. L. Efros, S. C. Erwin, *Science*, 2008, **319**, 1776; (c) F. Esch, S. Fabris, L. Zhou, T. Montini, C. Africh, P. Fornasiero, G. Comelli, R. Rosei, *Science*, 2005, **309**, 752.
- 3 (a) S. Y. Chung, S. Y. Choi, T. Yamamoto, Y. Ikuhara, *Phys. Rev. Lett.*, 2008, **100**, 125502; (b) S. Y. Chung, S. Y. Choi, T. Yamamoto, Y. Ikuhara, *Angewandte Chemie.*, 2009, **48**, 543.
- 4 (a) A. K. Padhi, K. S. Nanjundaswamy, J. Goodenough, *J. Electrochem. Soc.*, 1997, **144**, 1188; (b) A. Yamada, S. C. Chung, H. Hinokuma, *J. Electrochem. Soc.*, 2001, **148**, A224; (c) S.-Y. Chung, J. T. Bloking, Y.-M. Chiang, *Nat. Mater.*, 2002, **1**, 123; (d) M. S. Whittingham, Y. Song, S. Lutta, P. Y. Zavalij, N. A. Chernova, *J. Mater. Chem.*, 2005, **15**, 3362; (e) M. K. Devaraju, I. Honma, I. *Adv. Energy. Mater.*, 2012, **2**, 284; (f) M. K. Devaraju, Q. D. Truong, T. Tomai, H. Hyodo, I. Honma, *RSC Adv.*, 2014, **4**, 27452.
- 5 (a) J. Wolfenstine, J. Read, J. & J. L. Allen, *J. Power Sources*, 2007, **163**, 1070; (b) M. K. Devaraju, D. Rangappa, I. Honma, *Electrochimica Acta*, 2012, **85**, 548; (c) Q. D. Truong, M. K. Devaraju, T. Tomai, I. Honma, *ACS Appl.mater. Interfaces*, 2013, **5**, 9926; (d) Q. D. Truong, M. K. Devaraju, T. Tomai, I.

- Honma, *Scientific Reports*. 2014, **4**, 3975; (e) M. K. Devaraju, Q. D. Truong, H. Hyodo, T. Tomai, I. Honma, *Inorganics*, 2014, **2**(2), 233.
- 6 M. K. Devaraju, Q. D. Truong, I. Honma, *RSC Adv.*, 2013, **3**(43), 20633.
- 7 Q. D. Truong, M. K. Devaraju, Y. Sasaki, H. Hyodo, T. Tomai, I. Honma, *Chem. Mater.*, 2014, **26**, 2770.
- 8 (a) L. Gu, C. Zhu, H. Li, Y. Yu, C. Li, S. Tsukimoo, J. Maier, Y. Ikuhara, *J. Am. Chem. Soc.*, 2011, **133**, 4661; (b) X. Lu, Y. Sun, Z. Jian, X. He, L. Gu, Y. S. Hu, H. Li, Z. Wang, W. Chen, X. Duan, C. Li, J. Maier, S. Tsukimoto, Y. Ikuhara, *Y. Nano Lett.*, 2012, **12**, 6192.
- 9 S. Y. Chung, S. Y. Choi, S. S. Lee, Y. Ikuhara, *Y. Phys. Rev. Lett.*, 2012, **108**, 195501.
- 10 (a) D. Morgan, A. Van der Ven, G. Ceder, *Solid-State Lett.*, 2004, **7**, A30; (b) L. Laffont, C. Delacourt, P. Gibot, M. Y. Wu, P. Kooyman, C. Masquelier, J. M. Tarascon, *Chem. Mater.*, 2006, **18**, 5520; (c) G. Chen, X. Song, J. T. Richardson, *Solid-State Lett.*, 2006, **9**, A295; (d) R. Amin, P. Balaya, J. Maier, *Solid-State Lett.*, 2007, **10**, A13. e) S.-I. Nishimura, G. Kobayashi, K. Ohoyama, R. Kanno, M. Yashima, A. Yamada, *Nat. Mater.*, 2008, **7**, 707; (f) J. Li, W. Yao, S. Martin, D. Vaknin, *Solid State Ionics.*, 2008, **179**, 2016.
- 11 (a) D. W. Han, Y. M. Kang, R. Z. Yin, M. S. Song, H. S. Kwon, *Electrochem. Commun.*, 2009, **11**, 137; (b) J. Liu, T. E. Conry, X. Y. Song, L. Yang, M. M. Doeff, T. J. Richardson, *J. Mater. Chem.*, 2011, **21**, 9984; (c) T. N. L. Doan, I. Taniguchi, *J. Power Sources.*, 2011, **196**, 5679.
- 12 K. Momma, F. Izumi, *J. Appl. Crystallogr.*, 2011, **44**, 1272-1276.

Graphical Abstract:



Antisite defects in cathode materials are important to understand the chemistry of cathode materials. Here in, we investigated the antisite defects in LiCoPO_4 nanocrystals synthesized via supercritical fluid process.